Perfect Crossed Andreev Reflection in Dirac Hybrid Junctions in the Quantum Hall Regime

Song-Bo Zhang[1] and Björn Trauzettel[1,2]
[1]Institute for Theoretical Physics and Astrophysics, University of Würzburg, D-97074 Würzburg, Germany
[2]Würzburg-Dresden Cluster of Excellence ct.qmat, Germany

(Received 30 January 2019; published 28 June 2019)

Perfect crossed Andreev reflection (CAR) is striking for high-efficiency Cooper pair splitting, which bears promising applications in quantum communication. Recent experimental advances have disclosed the way to explore CAR in Dirac fermion systems under ultrastrong magnetic fields. We develop a scattering approach to study quantum-Hall–superconductor–quantum-Hall junctions formed by a two-dimensional time-reversal symmetric Dirac semimetal. We propose two different setups of the hybrid junction in the quantum limit, where only zeroth Landau levels are involved in transport to exploit perfect CAR. In both setups, the CAR probability can reach unity without applying bias voltage and is controllable by the magnetic field strength, the junction width, the length, and the doping of the superconductor. CAR dominates the nonlocal transport and is directly measurable by the differential conductances. We also identify a quantized spin injection per CAR event in one of the two setups. Our proposal is experimentally feasible and will be helpful for exploring high-efficiency Cooper pair splitting and spin injection in Dirac materials.

DOI: 10.1103/PhysRevLett.122.257701

Introduction.—Crossed Andreev reflection (CAR) is a process of converting an electron (hole) from one lead to a hole (electron) in another lead through a superconductor (S) [1–3]. Via CAR, Cooper pairs, which are strongly entangled electron pairs, can in principle be split spatially [2–4]; and they find fundamental interest and promising applications in quantum communication [5–7]. Thus, searching for systems with a large probability and convenient manipulation of CAR is desirable. A variety of candidate systems for CAR have been proposed, which include ferromagnetic junctions [8–12]; p-n junctions [13,14]; topological systems [15–20]; and other platforms [21–33]. Some of them have been experimentally implemented [9,21–29]. Nevertheless, most proposals require a fine-tuning of the electronic structure or a particular bias voltage. Usually, the processes of electron cotunneling (EC) and local Andreev reflection (LAR) are inevitable, which tend to suppress and obscure CAR. It remains a challenge to have a system free of both detrimental processes.

The quantum Hall (QH) effect forces charged carriers to move along chiral edge channels that are robust against disorder [34,35]. Recently, hybrid systems cooperating with the QH effect and superconductivity have been fabricated based on graphene [36–41] whose the low-energy physics is governed by Dirac fermions. This paves a new way to explore CAR in Dirac materials. However, many physical properties of Dirac hybrid structures in the QH regime, particularly in the quantum limit where only the lowest Landau levels contribute to transport, have yet to be explored.

In this Letter, we develop a scattering approach to investigate superconducting hybrid junctions in the QH regime, which are based on 2D time-reversal symmetric Dirac semimetals. In the quantum limit, the transport of the Dirac semimetal is governed by particular zeroth Landau levels that are spin polarized and chiral. Making use of this mechanism, we propose the quantum Hall–superconductor–quantum-Hall (QH-S-QH) junction in two different setups of the quantum limit as a novel platform for perfect CAR. One setup is a p-S-n junction with the same magnetic field but different types of doping in the two QH regions, whereas the other one is an n-S-n junction with opposite magnetic fields but the same type of doping, as sketched in Figs. 1(a) and (b), respectively. Remarkably, in both setups, EC and LAR are completely blocked; and CAR can be enhanced without fine-tuning of the bias voltage. The CAR probability can reach unity and is influenced by the length and doping of the superconductor, the magnetic field strength, and the junction width. Due to the particular properties of conducting channels, CAR dominates the nonlocal transport and can be directly measured by differential conductances. Moreover, we find that, while there is no spin injection in the n-S-n junction, a quantized spin injection per CAR event occurs in the p-S-n junction, which suggests a new route for high-efficiency spin injection in superconducting spintronics.

QH-S-QH *junction based on a 2D Dirac semimetal.*—We start with a time-reversal symmetric Dirac semimetal in two dimensions, which is described at low energies by

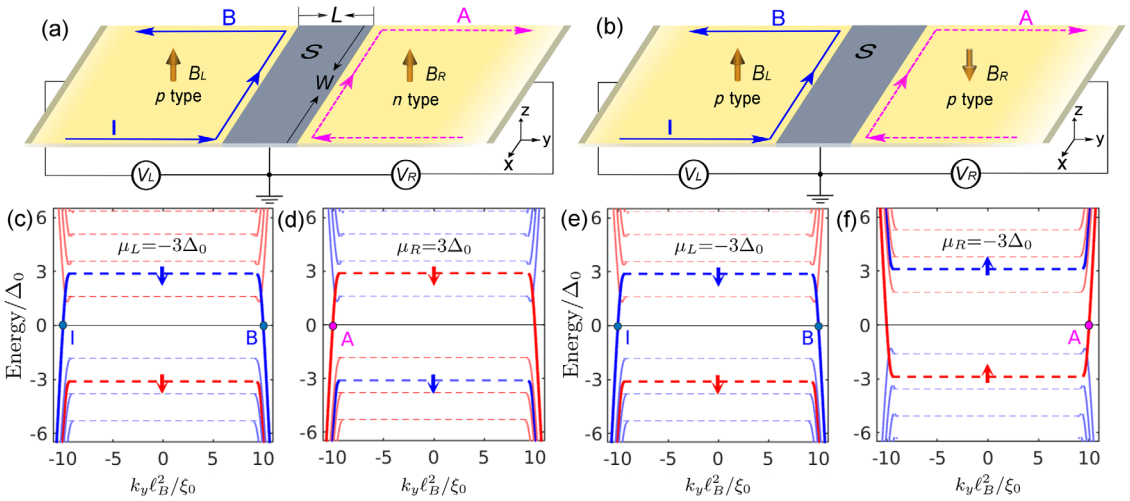

FIG. 1. (a) p-S-n junction with $\mu_L\mu_R<0$ and $B_LB_R>0$. Note that "n-type" and "p-type" refer to electron and hole doping, respectively. Excitation energy spectra in the (c) left and (d) right QH regions. Red and blue lines are for electrons and holes, respectively. The thick lines are zeroth Landau levels. Arrows $\uparrow(\downarrow)$ indicate spin-up(-down) polarization. The dashed lines represent the bulk Landau levels given by Eq. (4). Locations of the incident electron (I), normal reflected electron (B), and crossed-Andreev-reflected hole (A) are indicated in (a). Here, $\mu_R=-\mu_L=3\Delta_0$, $B_L=B_R=11B_0$, $\kappa=0.01v\xi_0$, and $W=20\xi_0$. (b) n-S-n junction with $\mu_L\mu_R>0$ and $B_LB_R<0$. (e) and (f) are the same as (c) and (d), but for the n-S-n junction with $\mu_R=\mu_L=-3\Delta_0$ and $B_L=-B_R=11B_0$.

$$H_0(\hat{\mathbf{k}})=\begin{pmatrix} H(\hat{\mathbf{k}}) & 0 \\ 0 & \mathcal{T}H(\hat{\mathbf{k}})\mathcal{T}^{-1}\end{pmatrix}. \tag{1}$$

The basis function is $(\psi_{+,\uparrow},\psi_{+,\downarrow},\psi_{-,\uparrow},\psi_{-,\downarrow})$, with the indices $\pm$ labeling the two Dirac cones related by time-reversal symmetry and $\uparrow,\downarrow$ labeling the two spins. The effective Hamiltonian reads $H(\hat{\mathbf{k}})=v\hat{k}_xs_x+v\hat{k}_ys_y+\kappa\hat{\mathbf{k}}^2s_z$, with v as the Fermi velocity, $\hat{\mathbf{k}}=(\hat{k}_x,\hat{k}_y)\equiv-i(\partial_x,\partial_y)$ as the wave vector operators, and (s_x,s_y,s_z) as the Pauli matrices acting on spin space. A small quadratic correction $\kappa|\mathbf{k}|\ll v$ is introduced to regulate the topological properties as $\mathbf{k}\to\infty$ and ensure definite edge states [42]. $\mathcal{T}=is_y\mathcal{C}$ is the time-reversal operator with $\mathcal{C}$ as the complex conjugation. Model (1) can be used to describe the surface states of 3D topological insulators [43–46], as well as the transition phase between a quantum spin Hall insulator and a normal insulator [47–49].

The QH-S-QH junction under study is formed by the Dirac semimetal in a strip geometry, as depicted in Figs. 1(a) and 1(b). Without loss of generality, we take the junction in the $\hat{y}$ direction and apply the magnetic field $B_{L/R}$ in the $\hat{z}$ direction in the left or right normal-metal lead. The junction (or strip) width is W, and the length of the S region is L. We consider s-wave superconductivity, which is induced locally by the proximity effect [50–53]. Then, the junction can be described by two decoupled sets of Bogoliubov-de Gennes (BdG) equations. The one acting on the basis $\Psi(\mathbf{r})=(\psi_{+,\uparrow},\psi_{+,\downarrow},\psi^\dagger_{-,\downarrow},-\psi^\dagger_{-,\uparrow})^T$ reads

$$\begin{pmatrix} H(\hat{\mathbf{K}})-\mu(\mathbf{r}) & \Delta(\mathbf{r}) \\ \Delta^*(\mathbf{r}) & \mathcal{T}H(-\hat{\mathbf{K}})\mathcal{T}^{-1}+\mu(\mathbf{r})\end{pmatrix}\Psi(\mathbf{r})=E\Psi(\mathbf{r}), \tag{2}$$

where the gate-voltage-tunable chemical potential $\mu(\mathbf{r})$ is assumed to vary stepwise, $\mu(\mathbf{r})=\mu_S$ in S ($|y|\le L/2$), and $\mu(\mathbf{r})=\mu_{L/R}$ in the left or right QH region ($|y|>L/2$). $\Delta(\mathbf{r})=\Delta_0\Theta(L/2-|y|)$ with $\Theta(y)$ as the Heaviside function is the pairing potential. It couples electron and hole excitations from different Dirac cones of time-reversal partners. The magnetic fields are taken into account via the vector potential $\boldsymbol{A}(y)=-yB_L\Theta(-y-L/2)\hat{x}-yB_R\Theta(y-L/2)\hat{x}$, and we substitute the wave vector operators as $\hat{\mathbf{K}}=\hat{\mathbf{k}}-e\mathbf{A}(\mathbf{r})/\hbar$ [54], where $e<0$ is the elementary charge. The other BdG equation acting on the basis $(\psi_{-,\uparrow},\psi_{-,\downarrow},\psi^\dagger_{+,\downarrow},-\psi^\dagger_{+,\uparrow})^T$ takes the same form as Eq. (2) but replaces κ by $-\kappa$.

Scattering approach.—In the QH-S-QH junction, the simple method of wave function matching to study transport [55] is no longer applicable. Hence, we need to generalize the scattering approach [56] for Dirac fermions under strong magnetic fields. We assume hard-wall boundary conditions in the $\hat{x}$ direction. In the QH regions, we expand the electron wave function by a complete set of quantum-well states

$$\Psi^\Lambda(\mathbf{r})=e^{ik_yy-ieB_\Lambda xy/\hbar}\sum_{j=1}^{\infty}\chi_j(x)f_j, \tag{3}$$

where $\chi_j(x)=\sqrt{2/W}\sin[j\pi(x/W+1/2)]$ for $|x|\le W/2$, and 0 otherwise. Note that f_j are spinors with only electron components in the basis used in Eq. (2). The phase factor $e^{-ieB_\Lambda xy/\hbar}$ stems from the gauge transformation from $\mathbf{A}=xB_\Lambda\hat{y}$ to $-yB_\Lambda\hat{x}$. $\Lambda\in\{L,R\}$ distinguishes the left and right QH regions. Plugging Eq. (3) into the BdG equation,

making use of the inner products between the $\chi_j(x)$, and then solving an eigenequation [57], we obtain the allowed k_y and f_j for a given E. The real solutions of k_y correspond to propagating channels. All the real k_y together form the excitation energy spectrum of (quasi)particles. Similarly, we find the basis wave function for holes by taking into account the phase factor $e^{ieB_\wedge xy/\hbar}$ and only hole components in f_j. In S, the electron and hole components are mixed, and the wave function is expanded in terms of $\chi_j(x)$ but without a phase factor.

With the solutions of a wave function in each individual region, we construct the scattering states in the junction. The expansion coefficients that measure scattering amplitudes between incident and outgoing channels are found by matching the wave function of the scattering state and its derivative at the QH-S interfaces. Summing the squared absolute values of the corresponding scattering amplitudes associated with propagating channels and normalized by the channel velocities, we finally obtain the probabilities of normal reflection (NR) R_{ee}, LAR R_{eh}, EC T_{ee}, and CAR T_{eh} [57].

Landau level spectra in the QH regions.—We analyze the energy spectra in the QH regions, which can provide helpful insights into the transport properties of the junction and the search for perfect CAR. In the QH regions, the energy spectra for electrons and holes are decoupled and formed by a series of discrete Landau levels. The guiding centers of electron and hole wave functions are determined by $x = \pm\hbar k_y/eB$, respectively. The Landau levels are flat when they are away from the edges at $x = \pm W/2$. In the limit $\kappa \ll v\sqrt{\hbar/|eB|}$, which corresponds to a small quadratic term in Eq. (1), the Landau levels in the bulk are given by

$$E_{\nu\pm} = \pm v\sqrt{2\nu|eB|/\hbar}, \qquad \nu = 1, 2, \ldots, \tag{4a}$$

$$E_0 = 0. \tag{4b}$$

The energies are measured from the Fermi level μ. These Landau levels can be found alternatively exploiting ladder operators [58,59]. In contrast, when close to the edges, all Landau levels exhibit finite dispersion. The positive levels $E_{\nu+}$ bend upward, whereas the negative levels $E_{\nu-}$ bend downward when approaching the edges. This behavior implies that electrons and holes move only in chiral channels close to the edges with their velocities given by $dE_{v\pm/0}/dk_y$. Interestingly, both the zeroth Landau levels of electrons and holes E_0, which are particular for the Dirac fermions, bend either upward or downward, depending on the magnetic field direction. Moreover, they have the same spin polarization, as indicated by the arrows in Figs. 1(c)–1(f), for which the direction also depends on the sign of the magnetic field. For $\mu = 0$, the Landau level spectra of electrons and holes coincide. A finite μ, however, shifts the spectra oppositely by $\mp\mu$. As a result, in the quantum limit $0 < |\mu| < v\sqrt{2|eB|/\hbar}$ [60], only a single chiral electron channel is maintained at the Fermi level and contributes to transport in one BdG block; whereas only a single chiral hole channel with opposite spin polarization contributes in the other block. Note that the two BdG blocks are completely decoupled in our system. The remarkable single-channel mechanism is unique to this hybrid junction, which is time-reversal symmetric in the absence of magnetic fields.

Perfect CAR.—The single-channel mechanism in the quantum limit (described above) is realized in two distinct setups of the QH-S-QH junction, namely, the p-S-n junction with $\mu_R\mu_L < 0$ and $B_LB_R > 0$ and the n-S-n junction with $\mu_R\mu_L > 0$ and $B_LB_R < 0$. In these setups, for a given BdG block, only electron channels are allowed in one QH region; whereas only hole channels are allowed in the other one. Thus, the processes of EC and LAR are completely suppressed. We are left with NR and CAR. If an electron stems from one Cooper pair in S and goes to one QH lead, then the other electron from the pair must go to the other lead. Note that these setups are the counterparts to junctions formed by helical liquids, where NR and CAR are forbidden [61,62]. As the chiral edge channels are topologically protected and prohibit backscattering, we expect the setups to be robust against weak disorder and nonideal conditions regarding interfaces and potential variations [63]. The two setups share many intriguing properties concerning CAR, which we discuss in the following.

We take the p-S-n junction for illustration. For definiteness, but without loss of generality, we assume a positive magnetic field $B_L = B_R \equiv B > 0$ and negative (positive) chemical potential in the left (right) QH region. Then, a single chiral electron channel exists in the left QH region, whereas a single antichiral hole channel exists in the right QH region. Thus, NR and CAR are cross-edge processes; i.e., the incident channels and reflected channels are at the different strip edges; see Figs. 1(a) and 1(b). To explore perfect CAR with $T_{eh} = 1$, we calculate and present in Fig. 2(a) the zero-energy probabilities of the four processes as functions of the length L. Here, we use Δ_0, $\xi_0 \equiv v/\Delta_0$, and $B_0 \equiv |\hbar/e\xi_0^2|$ as the units for energy, length, and the magnetic field, respectively. For the typical values of $v = 100\ \text{meV}\cdot\text{nm}$ (i.e., $v_F \equiv v/\hbar = 1.5 \times 10^5\ \text{m/s}a$) and $\Delta_0 = 1$ meV [64–66], we have $\xi_0 = 100$ nm and $B_0 = 0.066$ T, which are in an experimentally accessible regime. In the limit $L \to 0$, the system recovers an n-p junction, and electrons cannot be converted to holes due to the absence of superconductivity. In the opposite limit $L \gg \xi_0$, the tunneling across S is exponentially suppressed. Thus, $T_{eh} = 0$ as well. However, at intermediate length scales, we can find a large or even perfect CAR. Interestingly, the large CAR persists in the junction where the length L is longer than the superconducting coherence length ξ_0.

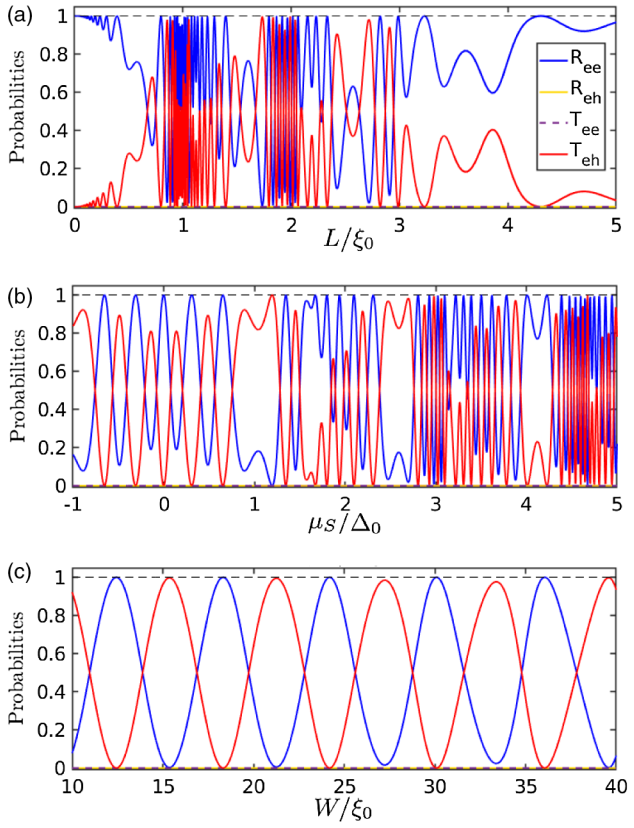

FIG. 2. Zero-energy probabilities of NR R_{ee} (blue), LAR R_{eh} (yellow), EC T_{ee} (purple), and CAR T_{eh} (red) as functions of (a) length L, (b) chemical potential μ_S, or (c) junction width W. Here, $B = 32B_0$, and other parameters for each panel are the same as in Fig. 3.

We also observe Fabry-Pérot oscillations with varying L, which stem from the interference effect in S with a finite μ_S. Fabry-Pérot oscillations also show up with respect to the doping μ_S of S and the magnetic field B; see Figs. 2(b) and 3(a). The interference occurs not only along the junction in $\hat{y}$ direction but also across the strip in the $\hat{x}$ direction. Thus, analogous oscillations appear with respect to the junction width W; see Fig. 2(c). The pattern of oscillations is, however, more regular because the interference consists of a single pair of propagating modes in the $\hat{x}$ direction, which is contrary to the interference in the $\hat{y}$ direction that also involves modes with decaying oscillation behavior. Therefore, we are able to obtain perfect CAR. It is possible to control CAR by the length, the doping of S, the magnetic field strength, and the junction width. Finally, we stress that the large CAR occurs at zero energy, which indicates the exemption from a fine-tuning of the bias voltage.

Next, we study the transport signature of CAR. We calculate the local and nonlocal differential conductances, which are defined as $G_{\mathrm{LL}} \equiv dI_L/dV_L|_{V_R=0}$ and $G_{\mathrm{LR}} \equiv dI_R/dV_L|_{V_R=0}$, respectively, by using the extended Blonder-Tinkham-Kapwijk theory [67,68]. Here, $I_{L/R}$ and $V_{L/R}$ are the measured current and the applied bias voltage in the left or right QH region, respectively. S is grounded. In the two setups, LAR and EC are eliminated completely so that NR and CAR dominate the local and nonlocal transports, respectively. The conductances at zero temperature are

$$G_{\mathrm{LR}} = -G_{\mathrm{LL}} = -(e^2/h)T_{eh}. \tag{5}$$

Here, $T_{eh} = 1 - R_{ee}$, as required by the particle conservation; and the bias voltage enters the conductances as excitation energy via T_{eh}. G_{LR} is negative and exactly opposite to G_{LL}, as shown in Fig. 3(b). Importantly, G_{LR} provides not only a transport signature but also a direct measurement of CAR.

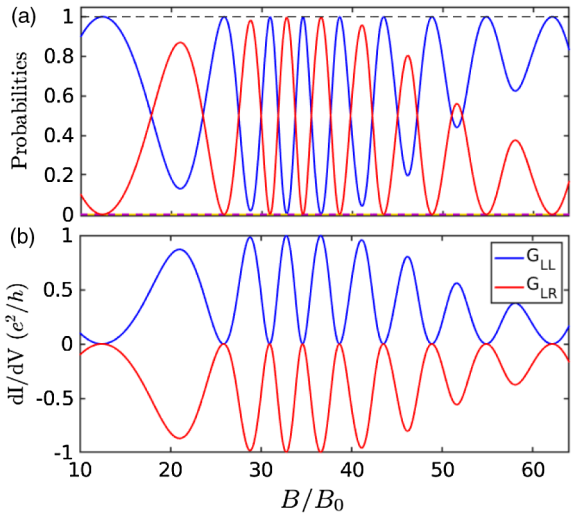

FIG. 3. (a) Zero-energy probabilities as functions of B in the quantum limit. Legend is the same as in Fig. 2(a). (b) Zero-bias local G_{LL} and nonlocal differential conductances G_{LR} as functions of B. We choose $L = 2\xi_0$, $W = 20\xi_0$, $\mu_S = \mu_R = -\mu_L = 3\Delta_0$, and $\kappa = 0.01v\xi_0$.

Spin injection in the p-S-n junction.—The difference of the two setups manifests mainly in the spin injection into S, which we now clarify. In the n-S-n junction, the incident electron and reflected hole carry opposite spin; see Figs. 1(e) and 1(f). This implies that two electrons with opposite spin are absorbed into S to form a spin-singlet Cooper pair, as we expect for s-wave superconductivity. Therefore, we have no spin transport between S and the QH regions.

However, this is not the case for the p-S-n junction. The reflected hole carries spin down, which is remarkably the same as that carried by the incident electron; see Figs. 1(c) and 1(d). To further confirm this, we calculate the density distributions of the four components of a scattering state near the junction in Fig. 4. In S, the four components mix together due the presence of superconductivity and strong spin-orbit coupling; and they oscillate in both $\hat{x}$ and $\hat{y}$ directions, reflecting the aforementioned interference effect. We see clearly that the incident electron carrying

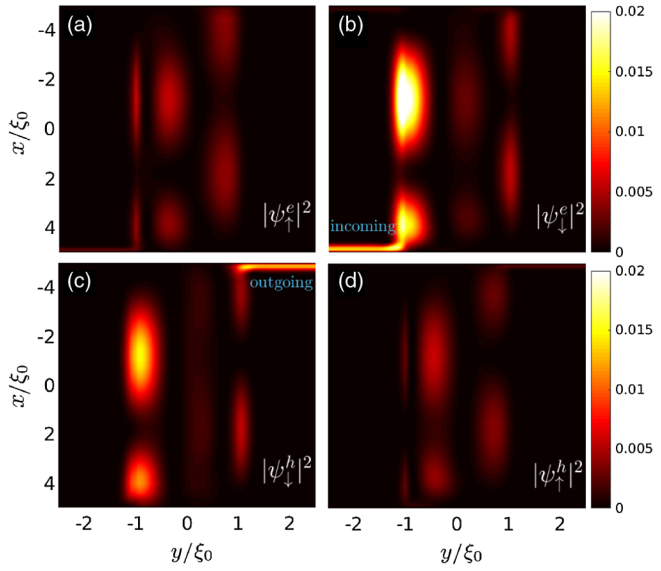

FIG. 4. Contour plots of the densities of (a) spin-up, (b) spin-down electrons, (c) spin-down, and (d) spin-up holes of a zero-energy scattering state in the p-S-n junction. Here, $B = 32B_0$, $W = 10\xi_0$, $L = 2\xi_0$, and other parameters are the same as in Fig. 3.

spin down at the lower edge is converted through S as a hole also carrying spin down at the upper edge into the other region. Therefore, we have an equal-spin CAR that effectively pumps two equal spins into S. The equal-spin CAR implies the creation of equal-spin triplet Cooper pairs in S [69–72], which are of interest in superconducting spintronics [73]. Following the approach of Ref. [70], we predict the value of spin pumped into S explicitly as

$$\bar{S}_z = -(h/2\pi)T_{eh}. \tag{6}$$

The spin injection is purely contributed by CAR. We have a quantized spin injection of $-h/2\pi$ per CAR event. For perfect CAR, we obtain a perfect spin injection.

Summary.—We have developed a scattering approach to investigate a 2D Dirac QH-S-QH junction. We have proposed two different setups, which exploit the particular properties of the zeroth Landau levels of the Dirac fermions in the quantum limit, for realizing high-efficiency and controllable CAR without fine-tuning of bias voltage. The differential conductances provide a direct measurement of CAR. We have identified a quantized spin injection in the p-S-n junction.

We thank C. Gould, L. W. Molenkamp, M. Stehno, and G. Tang for helpful discussions. This work was supported by the DFG (SPP1666 and SFB1170 "ToCoTronics"), the Würzburg-Dresden Cluster of Excellence ct.qmat (EXC2147, project-id 39085490), and the Elitenetzwerk Bayern Graduate School on "Topological Insulators".

[1] J. M. Byers and M. E. Flatté, Probing Spatial Correlations with Nanoscale Two-Contact Tunneling, Phys. Rev. Lett. **74**, 306 (1995).
[2] P. Recher, E. V. Sukhorukov, and D. Loss, Andreev tunneling, Coulomb blockade, and resonant transport of nonlocal spin-entangled electrons, Phys. Rev. B **63**, 165314 (2001).
[3] G. B. Lesovik, T. Martin, and G. Blatter, Electronic entanglement in the vicinity of a superconductor, Eur. Phys. J. B **24**, 287 (2001).
[4] P. Samuelsson, E. V. Sukhorukov, and M. Büttiker, Orbital Entanglement and Violation of Bell Inequalities in Mesoscopic Conductors, Phys. Rev. Lett. **91**, 157002 (2003).
[5] G. Burkard, D. Loss, and E. V. Sukhorukov, Noise of entangled electrons: Bunching and antibunching, Phys. Rev. B **61**, R16303 (2000).
[6] R. Horodecki, P. Horodecki, M. Horodecki, and K. Horodecki, Quantum entanglement, Rev. Mod. Phys. **81**, 865 (2009).
[7] K. Modi, A. Brodutch, H. Cable, T. Paterek, and V. Vedral, The classical-quantum boundary for correlations: Discord and related measures, Rev. Mod. Phys. **84**, 1655 (2012).
[8] G. Deutscher and D. Feinberg, Coupling superconducting-ferromagnetic point contacts by Andreev reflections, Appl. Phys. Lett. **76**, 487 (2000).
[9] D. Beckmann, H. B. Weber, and H. v. Löhneysen, Evidence for Crossed Andreev Reflection in Superconductor-Ferromagnet Hybrid Structures, Phys. Rev. Lett. **93**, 197003 (2004).
[10] J. Linder, M. Zareyan, and A. Sudbø, Spin-switch effect from crossed Andreev reflection in superconducting graphene spin valves, Phys. Rev. B **80**, 014513 (2009).
[11] K. Li and Y.-Y. Zhang, Spin-filtered and spatially distinguishable crossed Andreev reflection in a silicene-superconductor junction, Phys. Rev. B **94**, 165441 (2016).
[12] R. Beiranvand, H. Hamzehpour, and M. Alidoust, Nonlocal Andreev entanglements and triplet correlations in graphene with spin-orbit coupling, Phys. Rev. B **96**, 161403(R) (2017).
[13] J. Cayssol, Crossed Andreev Reflection in a Graphene Bipolar Transistor, Phys. Rev. Lett. **100**, 147001 (2008).
[14] M. Veldhorst and A. Brinkman, Nonlocal Cooper Pair Splitting in a $p\mathbf{S}n$ Junction, Phys. Rev. Lett. **105**, 107002 (2010).
[15] J. Nilsson, A. R. Akhmerov, and C. W. J. Beenakker, Splitting of a Cooper Pair by a Pair of Majorana Bound States, Phys. Rev. Lett. **101**, 120403 (2008).
[16] W. Chen, R. Shen, L. Sheng, B. G. Wang, and D. Y. Xing, Electron Entanglement Detected by Quantum Spin Hall Systems, Phys. Rev. Lett. **109**, 036802 (2012).
[17] W. Chen, R. Shen, L. Sheng, B. G. Wang, and D. Y. Xing, Resonant nonlocal Andreev reflection in a narrow quantum spin Hall system, Phys. Rev. B **84**, 115420 (2011).
[18] R. W. Reinthaler, P. Recher, and E. M. Hankiewicz, Proposal for an All-Electrical Detection of Crossed Andreev Reflection in Topological Insulators, Phys. Rev. Lett. **110**, 226802 (2013).
[19] J. J. He, J. Wu, T.-P. Choy, X.-J. Liu, Y. Tanaka, and K. T. Law, Correlated spin currents generated by resonant-crossed Andreev reflections in topological superconductors, Nat. Commun. **5**, 3232 (2014).

[20] J. Wang, L. Hao, and K. S. Chan, Quantized crossed-Andreev reflection in spin-valley topological insulators, Phys. Rev. B **91**, 085415 (2015).
[21] S. Russo, M. Kroug, T. M. Klapwijk, and A. F. Morpurgo, Experimental Observation of Bias-Dependent Nonlocal Andreev Reflection, Phys. Rev. Lett. **95**, 027002 (2005).
[22] L. Hofstetter, S. Csonka, J. Nygård, and C Schönenberger, Cooper pair splitter realized in a two-quantum-dot Y-junction, Nature (London) **461**, 960 (2009).
[23] P. Cadden-Zimansky, J. Wei, and V. Chandrasekhar, Cooper-pair-mediated coherence between two normal metals, Nat. Phys. **5**, 393 (2009).
[24] J. Wei and V. Chandrasekhar, Positive noise cross-correlation in hybrid superconducting and normal-metal three-terminal devices, Nat. Phys. **6**, 494 (2010).
[25] L. G. Herrmann, F. Portier, P. Roche, A. L. Yeyati, T. Kontos, and C. Strunk, Carbon Nanotubes as Cooper-Pair Beam Splitters, Phys. Rev. Lett. **104**, 026801 (2010).
[26] J. Schindele, A. Baumgartner, and C. Schönenberger, Near-Unity Cooper Pair Splitting Efficiency, Phys. Rev. Lett. **109**, 157002 (2012).
[27] A. Das, Y. Ronen, M. Heiblum, D. Mahalu, A. V Kretinin, and H. Shtrikman, High-efficiency cooper pair splitting demonstrated by two-particle conductance resonance and positive noise cross-correlation, Nat. Commun. **3**, 1165 (2012).
[28] Z. B. Tan, D. Cox, T. Nieminen, P. Lähteenmäki, D. Golubev, G. B. Lesovik, and P. J. Hakonen, Cooper Pair Splitting by Means of Graphene Quantum Dots, Phys. Rev. Lett. **114**, 096602 (2015).
[29] G. Fülöp, F. Domínguez, S. d'Hollosy, A. Baumgartner, P. Makk, M. H. Madsen, V. A. Guzenko, J. Nygård, C. Schönenberger, A. Levy Yeyati, and S. Csonka, Magnetic Field Tuning and Quantum Interference in a Cooper Pair Splitter, Phys. Rev. Lett. **115**, 227003 (2015).
[30] Z. Hou, Y. Xing, A.-M. Guo, and Q.-F. Sun, Crossed Andreev effects in two-dimensional quantum Hall systems, Phys. Rev. B **94**, 064516 (2016).
[31] Y. S. Ang, L. K. Ang, C. Zhang, and Z. Ma, Nonlocal transistor based on pure crossed Andreev reflection in a EuO-graphene/superconductor hybrid structure, Phys. Rev. B **93**, 041422(R) (2016).
[32] M. Beconcini, M. Polini, and F. Taddei, Nonlocal superconducting correlations in graphene in the quantum Hall regime, Phys. Rev. B **97**, 201403(R) (2018).
[33] F. Finocchiaro, F. Guinea, and P. San-Jose, Topological π Junctions from Crossed Andreev Reflection in the Quantum Hall Regime, Phys. Rev. Lett. **120**, 116801 (2018).
[34] R. B. Laughlin, Quantized Hall conductivity in two dimensions, Phys. Rev. B **23**, 5632 (1981).
[35] B. I. Halperin, Quantized Hall conductance, current-carrying edge states, and the existence of extended states in a two-dimensional disordered potential, Phys. Rev. B **25**, 2185 (1982).
[36] P. Rickhaus, M. Weiss, L. Marot, and C. Schönenberger, Quantum Hall effect in graphene with superconducting electrodes, Nano Lett. **12**, 1942 (2012).
[37] F. Amet, C. T. Ke, I. V. Borzenets, J. Wang, K. Watanabe, T. Taniguchi, R. S. Deacon, M. Yamamoto, Y. Bomze, S. Tarucha, and G. Finkelstein, Supercurrent in the quantum Hall regime, Science **352**, 966 (2016).
[38] G.-H. Lee, K.-F. Huang, D. K. Efetov, D. S. Wei, S. Hart, T. Taniguchi, K. Watanabe, A. Yacoby, and P. Kim, Inducing superconducting correlation in quantum Hall edge states, Nat. Phys. **13**, 693 (2017).
[39] G.-H. Park, M. Kim, K. Watanabe, T. Taniguchi, and H.-J. Lee, Propagation of superconducting coherence via chiral quantum-Hall edge channels, Sci. Rep. **7**, 10953 (2017).
[40] M. R. Sahu, X. Liu, A. K. Paul, S. Das, P. Raychaudhuri, J. K. Jain, and A. Das, Inter-Landau-level Andreev Reflection at the Dirac Point in a Graphene Quantum Hall State Coupled to a $NbSe_2$ Superconductor, Phys. Rev. Lett. **121**, 086809 (2018).
[41] A. Seredinski, A. W. Draelos, E. G. Arnault, M.-T. Wei, H. Li, K. Watanabe, T. Taniguchi, F. Amet, and G. Finkelstein, Full control of quantum Hall supercurrent in a side gated graphene Josephson junction, arXiv:1901.05928.
[42] S. Q. Shen, *Topological Insulators: Dirac Equation in Condensed Matters* (Springer, Berlin, 2012).
[43] H. Zhang, C. X. Liu, X. L. Qi, X. Dai, Z. Fang, and S. C. Zhang, Topological insulators in Bi_2Se_3, Bi_2Te_3 and Sb_2Te_3 with a single Dirac cone on the surface, Nat. Phys. **5**, 438 (2009).
[44] Y. L. Chen, J. G. Analytis, J. H. Chu, Z. K. Liu, S. K. Mo, X. L. Qi, H. J. Zhang, D. H. Lu, X. Dai, Z. Fang, S. C. Zhang, I. R. Fisher, Z. Hussain, and Z. X. Shen, Experimental realization of a three-dimensional topological insulator, Bi_2Te_3, Science **325**, 178 (2009).
[45] H. Z. Lu, W. Y. Shan, W. Yao, Q. Niu, and S. Q. Shen, Massive Dirac fermions and spin physics in an ultrathin film of topological insulator, Phys. Rev. B **81**, 115407 (2010).
[46] W. Y. Shan, H. Z. Lu, and S. Q. Shen, Effective continuous model for surface states and thin films of three-dimensional topological insulators, New J. Phys. **12**, 043048 (2010).
[47] B. A. Bernevig, T. L. Hughes, and S. C. Zhang, Quantum spin Hall effect and topological phase transition in HgTe quantum wells, Science **314**, 1757 (2006).
[48] S. Murakami, S. Iso, Y. Avishai, M. Onoda, and N. Nagaosa, Tuning phase transition between quantum spin Hall and ordinary insulating phases, Phys. Rev. B **76**, 205304 (2007).
[49] B. Büttner, C. X. Liu, G. Tkachov, E. G. Novik, C. Brüne, H. Buhmann, E. M. Hankiewicz, P. Recher, B. Trauzettel, S. C. Zhang, and L. W. Molenkamp, Single valley Dirac fermions in zero-gap HgTe quantum wells, Nat. Phys. **7**, 418 (2011).
[50] L. Fu and C. L. Kane, Superconducting Proximity Effect and Majorana Fermions at the Surface of a Topological Insulator, Phys. Rev. Lett. **100**, 096407 (2008).
[51] T. D. Stanescu, J. D. Sau, R. M. Lutchyn, and S. Das Sarma, Proximity effect at the superconductor–topological insulator interface, Phys. Rev. B **81**, 241310(R) (2010).
[52] D. Zhang, J. Wang, A. M. DaSilva, J. S. Lee, H. R. Gutierrez, M. H. W. Chan, J. Jain, and N. Samarth, Superconducting proximity effect and possible evidence for pearl vortices in a candidate topological insulator, Phys. Rev. B **84**, 165120 (2011).
[53] L. Maier, J. B. Oostinga, D. Knott, C. Brüne, P. Virtanen, G. Tkachov, E. M. Hankiewicz, C. Gould, H. Buhmann, and L. W. Molenkamp, Induced Superconductivity in the

Three-Dimensional Topological Insulator HgTe, Phys. Rev. Lett. **109**, 186806 (2012).

[54] We assume that the Zeeman splitting is small as compared to the energy scale of the spin-orbit coupling, and hence can be neglected. We also assume that the magnetic length is much larger than the Meissner penetration length, and we neglect the smoothing of interfaces.

[55] G. E. Blonder, M. Tinkham, and T. M. Klapwijk, Transition from metallic to tunneling regimes in superconducting microconstrictions: Excess current, charge imbalance, and supercurrent conversion, Phys. Rev. B **25**, 4515 (1982).

[56] H. Tamura and T. Ando, Conductance fluctuations in quantum wires, Phys. Rev. B **44**, 1792 (1991).

[57] See Supplemental Material at http://link.aps.org/supplemental/10.1103/PhysRevLett.122.257701 for the details of calculation.

[58] S. B. Zhang, Y. Y. Zhang, and S. Q. Shen, Robustness of quantum spin Hall effect in an external magnetic field, Phys. Rev. B **90**, 115305 (2014).

[59] S. B. Zhang, H. Z. Lu, and S. Q. Shen, Edge states and integer quantum Hall effect in topological insulator thin films, Sci. Rep. **5**, 13277 (2015).

[60] The chemical potential fluctuations of $\delta\mu$ can be tolerated as long as $\delta\mu \ll v\sqrt{2|eB|/\hbar}$.

[61] P. Adroguer, C. Grenier, D. Carpentier, J. Cayssol, P. Degiovanni, and E. Orignac, Probing the helical edge states of a topological insulator by Cooper-pair injection, Phys. Rev. B **82**, 081303(R) (2010).

[62] F. Crépin, P. Burset, and B. Trauzettel, Odd-frequency triplet superconductivity at the helical edge of a topological insulator, Phys. Rev. B **92**, 100507(R) (2015).

[63] The concrete influence of disorder on our results is an open question. We plan to numerically study it in the future, based on lattice models.

[64] I. Knez, R. R. Du, and G. Sullivan, Andreev Reflection of Helical Edge Modes in InAs/GaSb Quantum Spin Hall Insulator, Phys. Rev. Lett. **109**, 186603 (2012).

[65] M.-X. Wang, C. Liu, J. F. Xu, F. Yang, L. Miao, M.-Y. Yao, C. L. Gao, C. Shen, X. Ma, X. Chen, Z.-A Xu, Y. Liu, S.-C. Zhang, D. Qian, J.-F Jia, and Q.-K. Xue, The coexistence of superconductivity and topological order in the Bi_2Se_3 thin films, Science **336**, 52 (2012).

[66] J. Wiedenmann, E. Bocquillon, R. S. Deacon, S. Hartinger, O. Herrmann, T. M. Klapwijk, L. Maier, C. Ames, C. Brüne, C. Gould, A. Oiwa, K. Ishibashi, S. Tarucha, H. Huhmann, and L. W. Molenkamp, 4π-periodic Josephson supercurrent in HgTe-based topological Josephson junctions, Nat. Commn. **7**, 10303 (2016).

[67] C. J. Lambert, V. C. Hui, and S. J. Robinson, Multi-probe conductance formulae for mesoscopic superconductors, J. Phys. Cond. Matter **5**, 4187 (1993).

[68] M. P. Anantram and S. Datta, Current fluctuations in mesoscopic systems with Andreev scattering, Phys. Rev. B **53**, 16390 (1996).

[69] C. Benjamin, Crossed Andreev reflection as a probe for the pairing symmetry of ferromagnetic superconductors, Phys. Rev. B **74**, 180503(R) (2006).

[70] D. Breunig, P. Burset, and B. Trauzettel, Creation of Spin-Triplet Cooper Pairs in the Absence of Magnetic Ordering, Phys. Rev. Lett. **120**, 037701 (2018).

[71] C. Fleckenstein, N. Traverso Ziani, and B. Trauzettel, Conductance signatures of odd-frequency superconductivity in quantum spin Hall systems using a quantum point contact, Phys. Rev. B **97**, 134523 (2018).

[72] For Dirac fermions with a linear spectrum, the orbital effect of the magnetic field enters as a spatially varying vector potential and plays the role of an effective magnetization. Thus, the QH-*S*-QH junction behaves similarly to the ferromagnet-superconductor-ferromagnet junction. The interplay of the magnetization and spin-orbit interaction implies equal-spin triplet pairing near the interfaces.

[73] J. Linder and Jason W. A. Robinson, Superconducting spintronics, Nat. Phys. **11**, 307 (2015).